Journal of Materials Chemistry C

ROYAL SOCIETY OF CHEMISTRY

PAPER

View Article Online
View Journal | View Issue

Cite this: *J. Mater. Chem. C*, 2020, **8**, 17289

Suppressing π–π stacking interactions for enhanced solid-state emission of flat aromatic molecules *via* edge functionalization with picket-fence-type groups†

Hye Jin Cho,‡[a] Sang Won Kim,‡[b] Sungjin Kim,[c] Sangback Lee,[d] Juhyen Lee,[a] Yeonchoo Cho,[b] Yunmi Lee,[d] Tae-Woo Lee,[cef] Hyeon-Jin Shin[b] and Changsik Song*[a]

Received 14th September 2020,
Accepted 4th November 2020

DOI: 10.1039/d0tc04376a

rsc.li/materials-c

Polycyclic aromatic hydrocarbons (PAHs) are promising for materials science because of their high thermal and chemical stability, electron mobility, and unique photophysical properties. However, flat PAHs have limited applications owing to the low processability of their solutions, which originates from the strong π–π interaction between the aromatic rings. Herein, we report an effective method to suppress the π–π stacking of flat and large PAHs through steric hindrance. A 2,6-dimethylphenyl group, which is referred to as the "picket-fence" (PF) group based on its fence-like shape, was introduced on the edge of hexa-*peri*-hexabenzocoronene (HBC) through a bottom-up synthetic process. The PF group enhanced the solubility of HBC, while the unique photophysical properties of the core structure were preserved even in the solid state. The steric effect of the PF group is also demonstrated with other flat PAHs, which show excellent solid-state photophysical properties after functionalization with the PF group. Experimental and theoretical results indicate that the picket size plays a critical role in adjusting the PF effect. Furthermore, we fabricated the first organic light-emitting diode (OLED) that uses an HBC-based emitter, and the solid-state emission spectrum of the device is almost the same as that of the emitter in solution. This is possibly due to the maintenance of their morphology without aggregation due to the PF effect. Moreover, the full width at half maximum of the electroluminescence band was very narrow at only 20 nm.

Introduction

Flat polycyclic aromatic hydrocarbons (PAHs) have been intensively investigated over the past decade because all PAHs, from the smallest PAH (naphthalene) to extended molecules (*e.g.*, C222 arene),[1] have great potential in materials science owing to their intrinsic properties such as high thermal and chemical stabilities, outstanding ordered structures, and unique optoelectronic properties.[2–4] Conventionally, flat polycyclic aromatic compounds are applied in organic light-emitting diodes (OLEDs),[5–7] dyes,[8,9] optical sensors,[10–12] photovoltaic cells,[13–16] and field-effect transistors.[17,18] However, the strong π–π interaction between the aromatic cores hinders their processability because the stacked molecules are insoluble. Moreover, molecular stacking of flat PAHs is accompanied by undesirable changes in their photophysical properties.[19–21] Hitherto, numerous studies have aimed to improve the solution processability of large PAHs, especially that of hexa-*peri*-hexabenzocoronene (HBC). A popular method for fabricating soluble HBC is to functionalize the corona *via* bottom-up synthesis.[22–26] Although functionalized HBC derivatives show

[a] *Department of Chemistry, Sungkyunkwan University, 2066 Seobu-ro, Jangan-gu, Suwon-si, Gyeonggi-do, 16419, Republic of Korea. E-mail: songcs@skku.edu*
[b] *Inorganic Material Lab, Samsung Advanced Institute of Technology (SAIT), Samsung Electronics Co., Suwon 16678, Republic of Korea*
[c] *Department of Materials Science and Engineering, Seoul National University, Seoul 08826, Republic of Korea*
[d] *Department of Chemistry, Kwangwoon University, 20 Kwangwoon-ro, Nowon-gu, Seoul, 01897, Republic of Korea*
[e] *School of Chemical and Biological Engineering, Seoul National University, Seoul 08826, Republic of Korea*
[f] *Institute of Engineering Research, Research Institute of Advanced Materials, Nano Systems Institute (NSI), Seoul National University, Seoul 08826, Republic of Korea*

† Electronic supplementary information (ESI) available: Absorption and emission spectra of PF-functionalized PAHs; structure and information of single-crystal **HBC-PF6**; rotational barrier graphs; the simulated dimer structure of pyrene; determination of relative QY in solution; the HOMO and LUMO of **Py-Ph4** and **Py-PF4**; and experimental procedures for the synthesis of PAHs and their characterization. CCDC 2016559. For ESI and crystallographic data in CIF or other electronic format see DOI: 10.1039/d0tc04376a

‡ These authors contributed equally to this work.

meaningful enhancement in solubility, they are still prone to π–π stacking, especially in their solid state. Thus, only a few studies have reported the solid-state photophysical properties of HBC, which shows peak broadening or red-shifting of the absorption and emission spectra compared to the solution.[27–29]

Herein, we report the bottom-up synthesis and photophysical properties of a series of PAHs that have simple aromatic substituents on their edges. The 2,6-substituted phenyl group is termed the "picket-fence" (PF) group based on its fence-like shape[30] around the aromatic core. The PF groups tend to align vertically with respect to the plane of the aromatic core due to the high rotational barrier of the C–C bond between the PF group and the adjacent benzene ring of the core. Therefore, they can effectively suppress the stacking between two adjacent aromatic cores through steric hindrance in solution, and more importantly, in the solid state. The existence of PF-functionalized PAHs as individual molecules in solution was confirmed by the fine structure of their absorption and emission spectra. Furthermore, we demonstrate the effect of PF groups on the inhibition of π–π stacking through rotational barrier calculations and simulation data, as well as single-crystal X-ray crystallography. Moreover, we fabricated the first light-emitting device that uses an HBC-based emitter, termed **HBC-PF6**, with unchanged photophysical properties. This will provide a basis for future studies on the application of PAHs. We achieved an emission spectrum with a narrow bandwidth (full width at half maximum (FWHM) of 20 nm) and a maximum external quantum efficiency (EQE) of 1%.

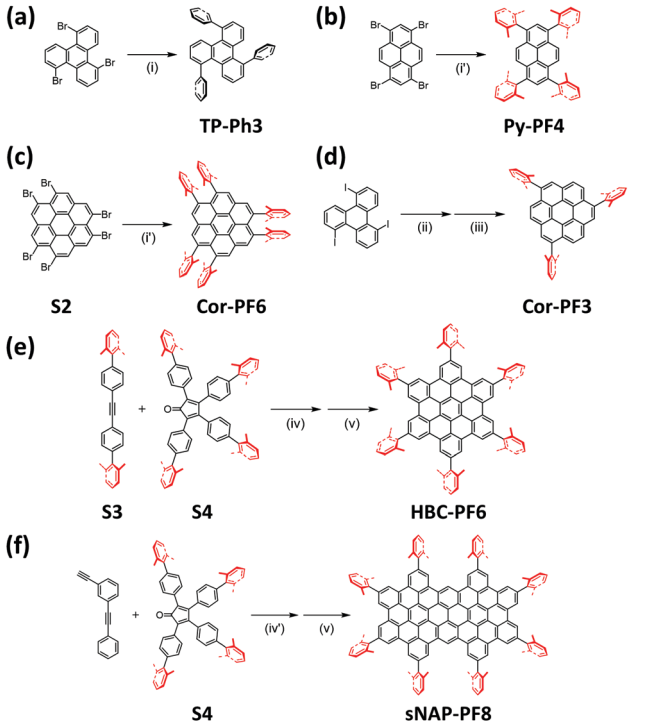

Scheme 1 Synthetic pathways of PF-functionalized PAHs: (a) **TP-Ph3**, (b) **Py-PF4**, (c) **Cor-PF6**, (d) **Cor-PF3**, (e) **HBC-PF6**, and (f) **sNAP-PF8**. Conditions: (i) $PhB(OH)_2$, $Pd(PPh_3)_4$, Cs_2CO_3, 1,4-dioxane/H_2O, 100 °C, 12 h. (i') PF-$B(OH)_2$, $Pd(PPh_3)_4$, Cs_2CO_3, 1,4-dioxane, reflux, 24 h. (ii) 2-ethynyl-1,3-dimethylbenzene, $Pd(PPh_3)_4$, CuI, Et_3N, THF, 70 °C, 12 h. (iii) $PtCl_2$, PhMe, 90 °C, 48 h. (iv) Ph_2O, reflux, 48 h. (iv') Ph_2O, reflux, 49 h. (v) $FeCl_3$, CH_2Cl_2/$MeNO_2$, room temperature, 2 h.

Results and discussion

PF-functionalized PAHs with various aromatic core structures (Scheme 1) were synthesized *via* bottom-up methods. We successfully synthesized **TP-Ph3**, **Py-PF4**, and **Cor-PF6** from bromo-substituted PAHs (triphenylene, TP; pyrene, Py; and coronene, Cor) by the Suzuki coupling reaction. Three other samples based on coronene (**Cor-PF3**), HBC (**HBC-PF6**), and supernaphthalene (sNAP) (**sNAP-PF8**) were synthesized by multi-step bottom-up procedures. The overall yields of the reactions were reasonable at >50%, except for that of **Cor-PF6** (11%). The synthesis procedures are given in detail in the ESI.†

Unlike other small PAHs, such as triphenylene, pyrene, and coronene, HBC is rarely soluble in common laboratory solvents. Fig. 1a compares the supernatant of the HBC/tetrahydrofuran (THF) dispersion with a clear solution of **HBC-PF6** in THF. Note that HBC dispersed in the supernatant was not molecularly separated; in fact, it was severely aggregated. When this mixture was passed through a syringe filter (pore size of 200 nm), it turned clear and almost no HBC was left in the solution, as confirmed by UV-vis absorption spectroscopy (Fig. S1, ESI†). On the other hand, **HBC-PF6** showed a remarkably improved solubility, and formed a clear solution in THF at 1 mM concentration (Fig. 1a). This notable increase in solubility was confirmed by the absorption spectra in Fig. 1b and Fig. S1–S2 (ESI†). The saturated solution of **HBC-PF6** in THF showed a dramatic increase in absorption (by ~28 000 times) compared to that of the supernatant of HBC.

The PF groups seemed to determine the solubility of the entire structure as they masked the core. The solubilities of **HBC-PF6** in six different solvents, namely 1,2-dichlorobenzene (1,2-DCB), cyclohexanone, dichloromethane (DCM), *N*-methyl-2-pyrrolidone (NMP), THF, and toluene, were determined according to a previous study[31] on the dispersion of HBC. Among them, cyclohexanone and THF appeared to be the best solvents, and the solubilities of **HBC-PF6** in these solvents are 1.57 wt% (15.1 mg mL^{-1}) and 1.04 wt% (9.3 mg mL^{-1}), respectively (Fig. 1c). This extraordinary improvement in solubility could be attributed to the PF group because the interaction of PF groups with solvent molecules overwhelms that of the core. Thus, **HBC-PF6** differs from the parent HBC, although its Hildebrand solubility parameter (Fig. 1c; ~21 $MPa^{1/2}$) seems to be comparable to those of HBC[31] and other graphitic materials.[32–34]

Furthermore, we observed the disappearance of the undesired photophysical changes in the solid state of **HBC-PF6**, which is an important issue for its practical use. The absorption and emission spectra of the **HBC-PF6** film appeared to be almost identical to those of the **HBC-PF6** solution, and all the spectra showed fine vibronic structures (Fig. 1d). After the transition from the solution to film, the maximum emission peak of **HBC-PF6** had shifted by only 2 nm, which is 98% lower than that of HBC (119 nm) (Fig. 1e). Overall, PF groups do not appear to modify the core structure, indicating that our strategy of appending HBC with PF groups is

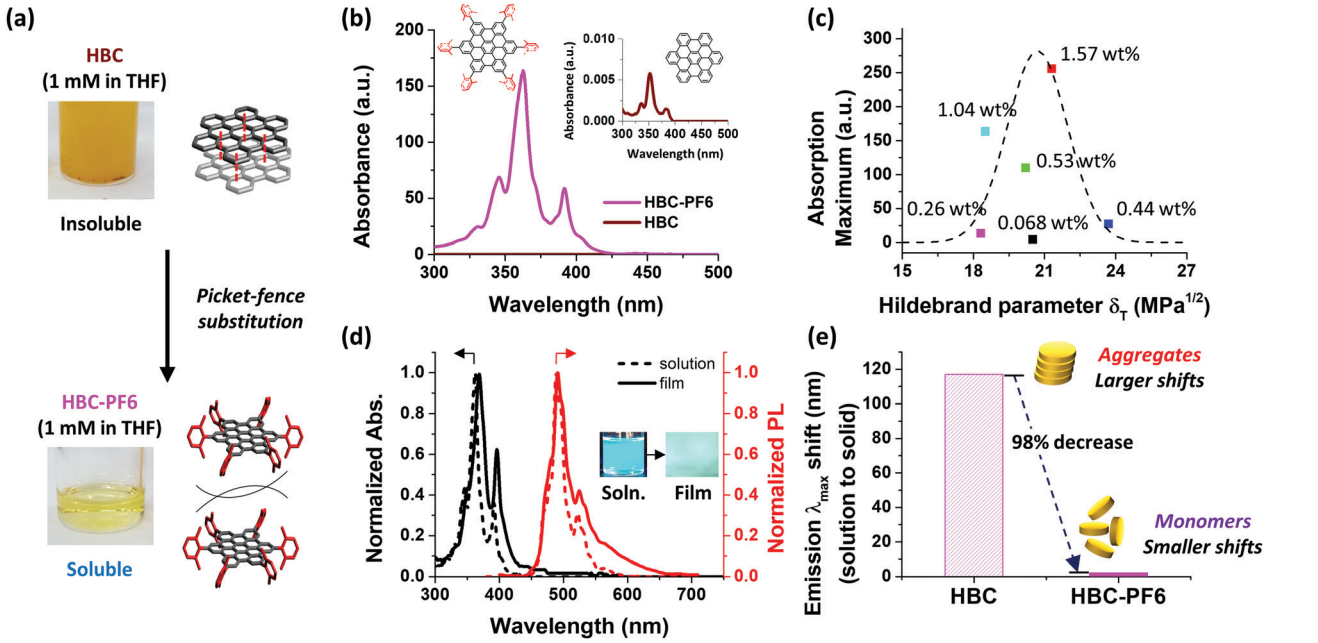

Fig. 1 Enhancement of the solubility of HBC by PF substitution. (a) HBC and **HBC-PF6** solutions in THF. (b) Absorption spectra of saturated solutions of HBC (*ca.* 2.5 × 10^{-7} M) and **HBC-PF6** in THF. (c) Absorption maxima of the saturated solutions of **HBC-PF6** as a function of the Hildebrand solubility parameter of the solvent (black: 1,2-dichlorobenzene; red: cyclohexanone; green: dichloromethane; blue: *N*-methyl-2-pyrrolidone; cyan: tetrahydrofuran; and magenta: toluene). (d) Absorption (black) and emission (red) spectra of **HBC-PF6** solution and film. The solutions (dashed line) were diluted with THF to the desired concentration of 3.0 × 10^{-7} M. Films (solid line) were prepared by spin-coating the stock solution (1.5 × 10^{-4} M in THF) on glass. (e) Shift in the maximum emission wavelengths of HBC and **HBC-PF6** in solutions compared to those of their films.

effective for achieving single-molecular characteristics of PAHs in the solid state. To evaluate our approach, we fabricated an OLED based on **HBC-PF6**, which is the first OLED that uses an HBC-based emitter. The electroluminescence (EL) spectrum of the OLED maintained the solution-like profile to an even greater extent than a thin film of **HBC-PF6** (details later).

We grew single crystals of **HBC-PF6** from a THF solution and analyzed the molecular structure by X-ray crystallography (Fig. 2a). **HBC-PF6** forms monoclinic crystals belonging to the $P2_1/c$ space group. The molecular structure of **HBC-PF6** is highly symmetric (Fig. S3a, ESI†). Hence, the six PF groups can be divided into three classes based on their dihedral angles. Each class of PF groups was tilted, but not orthogonally, with respect to the core, and the dihedral angles were in the 67.73°–72.66° range (Fig. S3b, ESI†). According to the molecular packing in the single crystal (Fig. 2b), the distance between two parallel planes containing the cores is 12.525 Å (Fig. S3c, ESI†), and the distance between the centers is 14.083 Å (Fig. S3d, ESI†). Thus, the separation between two adjacent molecules of **HBC-PF6** is very large, preventing intermolecular π–π interactions. The interplanar distance was much greater than that of the parent HBC or alkyl-substituted HBC,[35,36] and similar to that of permethoxylated HBC with a contorted structure.[37] This single-molecular property of **HBC-PF6** in the solid state resulted in excellent photophysical properties, as shown in Fig. 1d.

To investigate the origin of the PF effect, we performed rotational barrier calculations with several model compounds. Naphthalene (of the zigzag periphery) substituted with three different PF groups, namely phenyl, 2,6-dimethylphenyl, and 2,6-diisopropylphenyl groups, was used as a model compound for the calculations. The resulting rotational barrier increased with the picket size (Fig. 2c and Fig. S4, ESI†), as follows: –H (12.6 kcal mol^{-1}), $-CH_3$ (48.5 kcal mol^{-1}), and $-CH(CH_3)_2$ (68.8 kcal mol^{-1}). Even a methyl group was enough to cause the PF group to have a dihedral angle of 90° with respect to the plane of the adjacent phenyl ring in the lowest energy state (Fig. S5, ESI†).

The controlled PF effect was further confirmed with simulations on PAH dimerization. First principles simulations (using the Perdew–Burke–Ernzerhof (PBE) functional and 6-31G* basis set) were performed to detect the most stable stacking structures of pyrene, **Py-Ph4**, and **Py-PF4** (Fig. 2d and Fig. S7, ESI†). The results of simulations indicate that the PF group is better than the phenyl group (**Py-Ph4**) in preventing π–π stacking, because it increased the π–π stacking distance from 3.4 Å (pyrene) to 5.0 Å (**Py-PF4**).

A series of PF-functionalized PAHs were prepared to prove that the PF effect can be applied to various core structures. As the core size increased, the absorption and emission maxima varied from 258 to 428 nm and from 354 and 538 nm, respectively (dashed lines of Fig. 3a–d and Fig. S9; see also Fig. S10, ESI†). Interestingly, we obtained the absorption and emission spectra of supernaphthalene for the first time by appending it with PF groups (**sNAP-PF8**) (Fig. 3d).

Next, PAH thin films were produced by spin-coating the stock solutions of each sample on glass substrates (Fig. 3e). The colors of the films under UV light (λ = 365 nm) varied from blue to orange with an increase in the core size. Excimer formation,

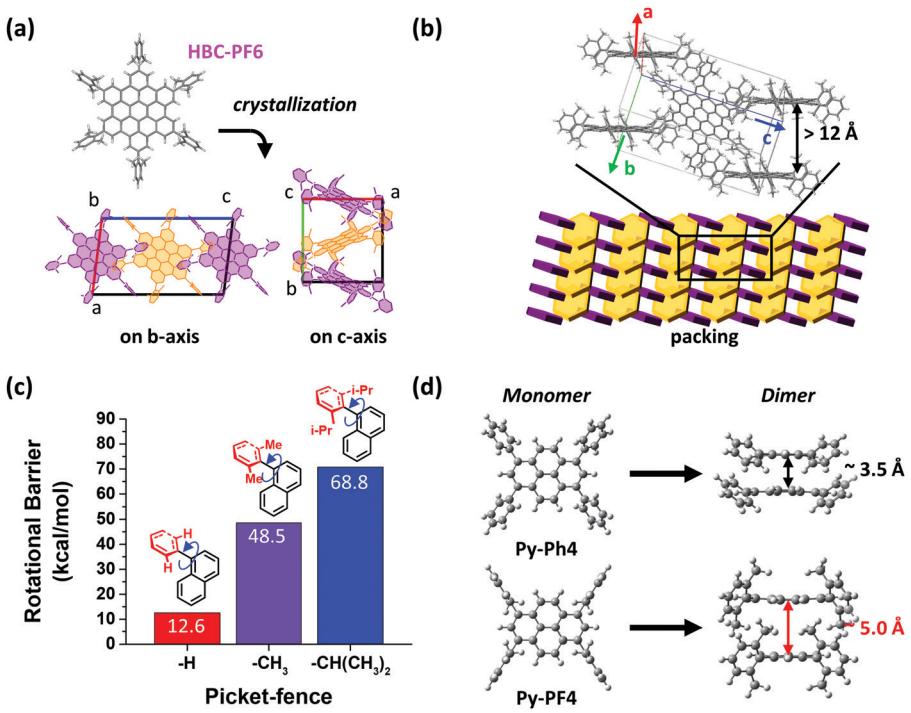

Fig. 2 (a) Molecular arrangement of three **HBC-PF6** molecules in a unit cell, viewed along the *b*- and *c*-axes. (b) Crystal packing of **HBC-PF6**; THF (solvent) molecules have been removed for clarity. (c) Rotational barrier calculated for three model compounds with different picket-fence structures (proton, methyl group, or isopropyl group). (d) Structures of the dimers of **Py-Ph4** and **Py-PF4**.

which is a typical solid-state photophysical characteristic of PAHs, was not observed. A vibronic fine structure appeared in the absorption and emission spectra of the thin films of PF-functionalized PAHs (solid lines of Fig. 3a–d and Fig. S9, ESI†), but not in the spectra of the pristine PAHs (Fig. S11, ESI†). Even **sNAP-PF8** could form emissive thin films with photophysical properties similar to those of its solution.

Similarly to the results for **HBC-PF6**, the other PF-functionalized PAHs exhibited a dramatic decrease in the red shift of emission bands between solutions and films. The red shifts are plotted in Fig. 3f, with the percentage decrement between the non-substituted and PF-functionalized PAHs indicated; the shift for the non-substituted PAH was taken as the standard for each core structure. The decrement varied from 75% to 98%.

The quantum yield (QY) values of the PF-functionalized PAHs (Fig. 3g and Table 1) were found to be significantly higher than those of the non-substituted PAHs. The QY of **Py-PF4** in solution is 21.6%, which is more than twice that of pyrene (9.4%). Such an increase in QY was also observed in coronene-based compounds; **Cor-PF6** showed a QY of 8.9%, whereas pristine coronene showed a QY of 2.0%. For HBC, which showed almost no emission, a slight increase to a QY of 3.1% was observed for **HBC-PF6**.

As the number of functionalized PF groups increased, the PAHs exhibited better properties (QY: coronene < **Cor-PF3** (6.3%) < **Cor-PF6**). We also obtained the QY values of PF-functionalized PAHs in their solid states, which is a first for large PAHs such as HBC or sNAP derivatives. The overall QY values of the films of PF-functionalized PAHs are either similar (**Cor-PF6**, **HBC-PF6**, and **sNAP-PF8**; Table 1, entries 8, 10, and 11) or slightly lower (**Py-PF4**; Table 1, entry 4) compared to those of their solutions.

According to the time-resolved photoluminescence measurements, the overall average fluorescence lifetimes (τ_{avg}) seem to decrease with the PF functionalization (Fig. S14, ESI†). It was observed that when compared to the unsubstituted PAHs (τ_{avg} = 8.7–342 ns), the PF-functionalized PAHs tend to have faster decay rate constants or shorter τ_{avg} (2.3–3.6 ns), probably due to the change in the vibrational mode related to the difference in the peripheral structure (C–H and C–PF). Interestingly, the thin film of **HBC-PF6** exhibited a similar emission decay curve to that of the solution but longer τ_{avg} (9.3 ns), because of the restricted vibrational motions in the solid state. From solution to film, the non-radiative decay rate decreased more than the radiative decay rate as the QY value of the film of **HBC-PF6** slightly increases (Table 1). For **sNAP-PF8**, each value of parameters appeared to be similar to relatively rigid samples.

On the other hand, the phenyl-substituted PAHs have excellent QY values of 69.9% (**TP-Ph3**) and 95.2% (**Py-Ph4**) in solution, but show a significant decrease to 14.6% (**TP-Ph3**) and 10.3% (**Py-Ph4**) as thin films. Unlike the phenyl rings, 2,6-dimethylphenyl groups seemed to have a less significant influence on the overall molecular energy levels. To confirm the influence of the substituents on the molecular orbital of the whole structures, we performed time-dependent density functional theory (TD-DFT) calculations after structural optimization of **Py-Ph4** and **Py-PF4** by employing the Gaussian09[38] suite of programs. The resulting highest occupied molecular orbital (HOMO) and lowest unoccupied molecular orbital (LUMO) of **Py-Ph4** and **Py-PF4** are shown in Fig. S8 (ESI†).

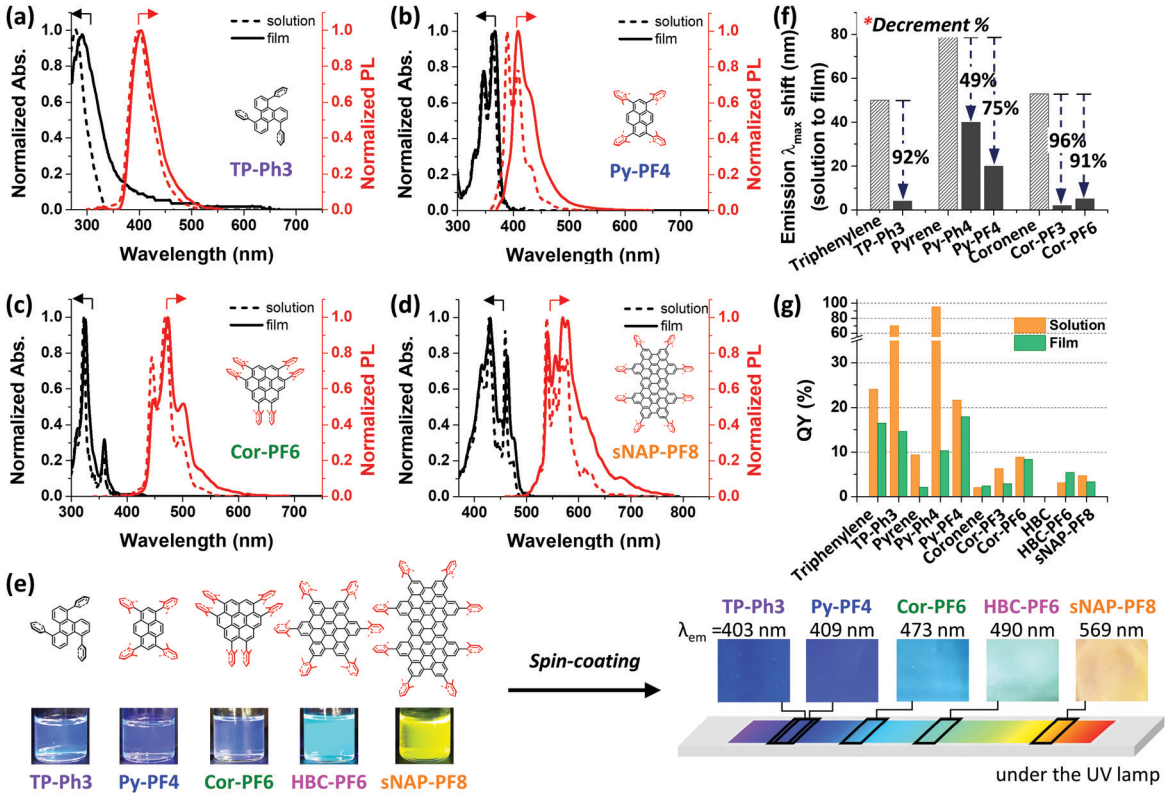

Fig. 3 Absorption (black) and emission (red) spectra of PF-functionalized PAHs: (a) **TP-Ph3**, (b) **Py-PF4**, (c) **Cor-PF6**, and (d) **sNAP-PF8**. THF (dashed line) were used for solutions of **Py-PF4** (1.0×10^{-6} M), **Cor-PF6** (3.0×10^{-7} M), and **sNAP-PF8** (3.3×10^{-7} M). Cyclohexane was used for **TP-Ph3** (1.0×10^{-6} M). Films (solid line) were prepared by using the stock solutions of **TP-Ph3** (9.0×10^{-4} M), **Py-PF4** (6.7×10^{-4} M), **Cor-PF6** (1.5×10^{-4} M), and **sNAP-PF8** (3.0×10^{-4} M) in THF. (e) Schematic representation of thin film formation from solutions (1.0×10^{-3} M for **TP-Ph3**, **Py-PF4**, **Cor-PF6**, and **HBC-PF6**; 2.0×10^{-4} M for **sNAP-PF8**). (f) Shifts in the emission maxima of unsubstituted and PF-functionalized PAHs when their solutions change into films (solid bar: PF-functionalized PAHs; line-patterned bar: unsubstituted PAHs). Comparisons between the PAHs are expressed in %. (g) Quantum yield (QY) of PAHs in solution (THF) and thin films.

Table 1 Absorption, emission maxima, and emission quantum yield (QY) of PF-functionalized PAHs in solution (soln) and as thin films

		Abs		PL			Φ (%)	
Entry	Derivative	λ_{max} soln/ nm	λ_{max} film/ nm	λ_{max} soln/ nm	λ_{max} film/ nm	Shift[a]/ nm	Soln[b]	Film[c]
1	Triphenylene	258	—	354	404	50	24.1	16.5
2	**TP-Ph3**	279	289	399	403	4	69.9	14.6
3	Pyrene	336	—	394	473	79	9.4	2.1
4	**Py-Ph4**	383	402	419	437, 459	40	95.2	10.3
5	**Py-PF4**	361	368	389	409	20	21.6	17.9
6	Coronene	303	309	446	499	53	2.0	2.4
7	**Cor-PF3**	312	318	456	458	2	6.3	2.9
8	**Cor-PF6**	323	324	468	473	5	8.9	8.4
9	HBC	352	—	481	—	119[d]	—	—
10	**HBC-PF6**	362	369	488	490	2	3.1	5.4
11	**sNAP-PF8**	428	430	538	569	31	4.7	3.3

[a] When changing from solution to film. [b] Relative quantum yields measured in THF solutions. [c] Absolute quantum yields of films fabricated on quartz plates measured by an integrating sphere method. [d] Calculated using the excimer emission maximum of ~600 nm.

The phenyl rings of **Py-Ph4** in the optimized condition are slightly tilted by about 60° with respect to the plane of the pyrene core, whereas the 2,6-dimethylphenyl rings in **Py-PF4** maintained their orthogonal orientation. Thus, the interaction between the 2,6-dimethylphenyl rings and pyrene core was small, and 2,6-dimethylphenyl rings were not considered to be part of the main chromophore.[39,40] This difference is revealed in the HOMO and LUMO energies; thus, the contribution of the PF groups on the molecular orbital is much smaller in **Py-PF4**.

Finally, we fabricated an OLED with a structure of ITO/GraHIL/TCTA:TPBI:**HBC-PF6**/TPBI/LiF/Al [ITO:indium tin oxide; GraHIL: poly(3,4-ethylenedioxythiophene)–poly(styrenesulfonate) (PEDOT:PSS) co-polymer with a perfluorinated ionomer; TCTA: 4,4′,4″-tris(carbazol-9-yl)triphenylamine; TPBI: 1,3,5-tris(phenyl-2-benzimidazolyl)-benzene] (Fig. 4a).[41,42] As mentioned above, this device is the first OLED that uses an HBC-based emitter. Despite numerous studies on the photoluminescence (PL) characteristics of HBC, there have been no reports on actual devices manufactured with HBC or their EL characteristics. Interestingly, the obtained emission peak is almost the same as that of **HBC-PF6** in solution and as a thin film (Fig. 4b). Fig. 4c and d show the current density–voltage–luminance (*J*–*V*–*L*) characteristics and EQE values of the OLED. The current efficiency and EQE of the device are 2.59 cd A^{-1} and 1.23%, respectively, at a voltage of 4.2 V. The maximum luminance is 1243 cd m^{-2} at a current density 90.7 mA cm^{-2}. The OLED with **HBC-PF6** provides an EL peak at 490 nm with a low turn-on voltage of 3.8 V. Moreover, the FWHM of the EL spectrum is very narrow at

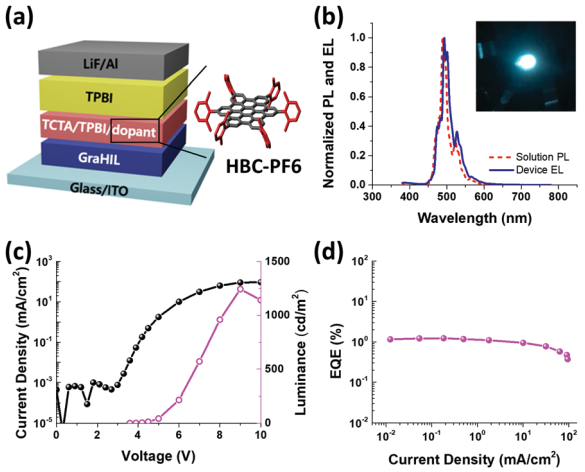

Fig. 4 Electrical and electroluminescence characteristics of an OLED based on **HBC-PF6**. (a) Architecture of the solution-processed OLED. (b) Electroluminescence spectrum of the OLED manufactured with **HBC-PF6** as the emitter, and its image (inset). (c) Current density *versus* voltage (left) and luminance *versus* voltage (right) curves. (d) EQE *versus* current density of the OLED.

~20 nm, presumably due to the prevention of π–π stacking between the HBC cores. Table S3 (ESI†) shows the device performances of PAH emitters with above 9 aromatic rings. Although the performances depend on the device architecture and optimization conditions, we can find the simple trend toward the broad FWHM and decreasing efficiency as the number of rings at the core increases. On the other hand, **HBC-PF6** shows a remarkable narrow FWHM and improved efficiencies compared to that of prior-arts.

Conclusions

In summary, we demonstrated that the picket-fence functionalization is a very effective strategy in developing solid-state emissive PAHs. In particular, we designed and synthesized edge-functionalized **HBC-PF6**, which has solution processability and outstanding single-molecular photophysical properties in the solid state. Although many groups have previously reported various methods for preventing π–π stacking, there was a lack of an in-depth study on the solid-state photophysical properties of the modified HBC. In order to prevent the π–π stacking of the HBC core through steric hindrance (*i.e.*, the PF effect), the methyl group was appropriate enough to exert the PF effect on the HBC core, although the PF effect is expected to be greater if the picket is bulkier. The single crystal structure of **HBC-PF6** proved that the large void placed between the molecules forbids them to be stacked, thus resulting in a large interplanar distance over 12 Å that is unprecedently large for planar HBC derivatives. Our study on the inhibition of the π–π stacking of HBC provides more profound insights into the processing of PAHs because it could be expanded on other flat PAHs such as triphenylenes, pyrenes, and coronenes with various core sizes and different peripheries. Our findings can serve as a foundation for further development of PAHs with a well-defined structure, better processability, and excellent properties. Furthermore, the first light-emitting device based on the HBC-based emitter provided almost the same emission spectrum as that of the solution, which is attributed to the prevention of molecular aggregation, and hence, the maintenance of the morphology of the emitter owing to the PF effect. Remarkably, the FWHM of the EL spectrum is very narrow at only 20 nm.

Experimental section

General information

Unless stated otherwise, all reactions were performed in vacuum-flame-dried glassware in an N_2 atmosphere using freshly distilled solvents. All starting materials and reagents were purchased from Sigma-Aldrich, Tokyo Chemical Industry Co., Ltd, Alfa Aesar, Samchun Pure Chemical, or Junsei Chemical Co., Ltd. The detailed information is given in synthesis detail in the ESI.† The commercial reagents were used without further purification.

The progress of the reaction was verified by thin-layer chromatography conducted with silica gel-coated glass slides using an F254 indicator. The compositions of the crude reaction mixture and synthesized products were first confirmed by NMR spectroscopy using a Bruker 500 MHz spectrometer. Tetramethylsilane was used as the internal standard, and chemical shifts (δ) are reported in parts per million relative to the peaks of residual solvents. Coupling constants (J) are expressed in hertz. High-resolution mass spectroscopy was conducted on a mass spectrometer (JEOL JMS-700). MALDI-TOF mass spectra were recorded on a Bruker UltrafleXtreme spectrometer using 7,7,8,8-tetracyanoquinodimethane (TCNQ) as the matrix. The details of the material preparation and characterization are included in the ESI.†

Evaluation of the photophysical properties

UV-vis absorption spectra were obtained using a UV-1800 (Shi-madzu) spectrophotometer at room temperature using a 1.0 cm quartz cell. Freshly distilled THF was used as the solvent. For all UV-vis measurements with solutions, the stock solutions of PAHs were diluted to the desired concentration.

Photoluminescence (PL) spectra were recorded on a Fluoro-Mate FS-2 (SCINCO) with the same samples used to obtain UV-vis absorption spectra. The excitation wavelength was varied according to the absorption maxima of the samples. Measurements were performed by tilting the film samples by 70° to prevent the reflectance of the incident light from the surface of the samples. Other factors including the lamp voltage and slit width were maintained constant during the measurements for the accurate comparison of the characteristics of each sample. The detailed measurement conditions about PL QY of solutions and solid film samples are described in the ESI.† Time-resolved PL characteristics for decay time of solution samples (**Py-PF4**, **Cor-PF6**, **HBC-PF6**, and **sNAP-PF8**) were measured using a time-correlated single photon counting (TCSPC) setup (Fluotime 300, PicoQuant GmbH). The samples were excited using a pulsed LED (PLS 340, Pico-Quant GmbH, 0.25 MHz repetition rate at 340 nm) at the Samsung Advanced Institute of Technology. For the other samples (HBC solution and the film of **HBC-PF6**), a picosecond pulsed laser with a laser head (LDH-P-C-405, PicoQuant GmBH, Berlin) driven by a PDL 800-B driver

(PicoQuant) was used as an excitation source (wavelength: 405 nm, pulse width: <70 ps, repetition rate: 5 MHz). The fluorescence was spectrally filtered using a monochromator (Acton SP-2150i, Princeton Instrument Inc., USA) and the time-resolved fluorescence signal was measured using a TCSPC module (PicoHarp, PicoQuant) combined with a microchannel plate photomultiplier tube (MCP-PMT, R3809U-59, Hamamatsu, Japan) at the Research Institute of Advanced Materials in Seoul National University.

Crystallographic data

Single crystals of **HBC-PF6** were grown by the slow evaporation of its THF solution. The crystal structures of the crystallized samples were determined by single-crystal diffraction methods at the Korea Basic Science Institute (KBSI, Western Seoul Center, Korea). A yellow crystal block ($0.39 \times 0.20 \times 0.09$ mm^3) was picked up with paratone oil and mounted on a Bruker D8 Venture PHOTON III M14 diffractometer equipped with a graphite-monochromated Mo Kα (λ = 0.71073 Å) radiation source and a nitrogen cold stream (−50 °C). Data collection and integration were performed with SMART APEX3 (Bruker, 2016) and SAINT (Bruker, 2016).[43,44] The absorption correction was performed by a multi-scan method implemented in SADABS.[43] The structure was solved by direct methods and refined by full-matrix least-squares on F^2 using SHELXTL.[45] All the non-hydrogen atoms were refined anisotropically, and the hydrogen atoms were added to their geometrically ideal positions.

Device fabrication

Patterned indium tin oxide (ITO)/glass substrates were cleaned by sequential sonication for 30 min each in acetone and isopropanol. Then, a 50–60 nm thick layer of GraHIL (a polymer blend of poly(3,4-ethylenedioxythiophene)–poly(styrenesulfonate)) (CLEVIOS P VP AI4083) and a tetra-fluoroethylene-perfluoro-3,6-dioxa-4-methyl-7-octenesulfonic acid co-polymer, CAS number: 31175-20-9, with a weight ratio of 1 : 3.6 was spin-coated on the cleaned ITO/glass substrate at 4500 rpm for 90 s to make a 50 nm thick GraHIL, and baked on a hot plate in air at 150 °C for 30 min. The other OLED layers were sequentially deposited on the GraHIL layer. A 40 nm thick emissive layer (EML) was spin-coated from a THF solution in a nitrogen glove box. The EML consisting of the 1 : 1 : 0.1 (w/w) mixture of a hole-transporting host (4,4′,4″-tris(carbazol-9-yl)triphenylamine; TCTA), an electron-transporting host (1,3,5-tri(phenyl-2-benzimidazolyl)-benzene; TPBI), and **HBC-PF6** dopants in tetrahydrofuran was then spin-coated on the GraHIL at 3000 rpm for 60 s and baked on a hot plate at 80 °C for 10 min. After the deposition of the EML, 50 nm thick TPBI was thermally deposited under high vacuum (5×10^{-7} torr) as an electron-transport layer. Finally, LiF (1 nm) and aluminum (100 nm) were sequentially deposited on the TPBI layer. The devices were finally encapsulated in a UV-curable epoxy resin.

Device characterization

The current–voltage–luminance characteristics were evaluated using a Keithley 236 source measurement unit and Minolta CS-2000 spectroradiometer.

Conflicts of interest

There are no conflicts to declare.

Acknowledgements

This work was supported by the Samsung Advanced Institute of Technology through the Samsung-SKKU Graphene/2D Center. It was also partially supported by the Nano Material Development Program through the National Research Foundation of Korea (NRF) funded by the Ministry of Education, Science and Technology (MEST), Republic of Korea (2012M3A7B4049644). The authors also thank Dr H. J. Lee (Western Seoul Center of Korea Basic Science Institute) for technical support with single-crystal X-ray crystallography.

References

1 C. D. Simpson, J. D. Brand, A. J. Berresheim, L. Przybilla, H. J. Rader and K. Müllen, *Chem. – Eur. J.*, 2002, **8**, 1424–1429.
2 A. Narita, X. Y. Wang, X. L. Feng and K. Müllen, *Chem. Soc. Rev.*, 2015, **44**, 6616–6643.
3 R. Rieger and K. Müllen, *J. Phys. Org. Chem.*, 2010, **23**, 315–325.
4 M. A. Sk, A. Ananthanarayanan, L. Huang, K. H. Lim and P. Chen, *J. Mater. Chem. C*, 2014, **2**, 6954–6960.
5 H. Jung, S. Kang, H. Lee, Y. J. Yu, J. H. Jeong, J. Song, Y. Jeon and J. Park, *ACS Appl. Mater. Interfaces*, 2018, **10**, 30022–30028.
6 S. L. Tao, Z. K. Peng, X. H. Zhang, P. F. Wang, C. S. Lee and S. T. Lee, *Adv. Funct. Mater.*, 2005, **15**, 1716–1721.
7 Y. H. Chung, L. Sheng, X. Xing, L. L. Zheng, M. Y. Bian, Z. J. Chen, L. X. Xiao and Q. H. Gong, *J. Mater. Chem. C*, 2015, **3**, 1794–1798.
8 S. Haldar, D. Chakraborty, B. Roy, G. Banappanavar, K. Rinku, D. Mullangi, P. Hazra, D. Kabra and R. Vaidhyanathan, *J. Am. Chem. Soc.*, 2018, **140**, 13367–13374.
9 G. T. Whiting, N. Nikolopoulos, I. Nikolopoulos, A. D. Chowdhury and B. M. Weckhuysen, *Nat. Chem.*, 2019, **11**, 23–31.
10 Z. Xu, N. J. Singh, J. Lim, J. Pan, H. N. Kim, S. Park, K. S. Kim and J. Yoon, *J. Am. Chem. Soc.*, 2009, **131**, 15528–15533.
11 A. Nierth, A. Y. Kobitski, G. U. Nienhaus and A. Jäschke, *J. Am. Chem. Soc.*, 2010, **132**, 2646–2654.
12 L. Ascherl, E. W. Evans, J. Gorman, S. Orsborne, D. Bessinger, T. Bein, R. H. Friend and F. Auras, *J. Am. Chem. Soc.*, 2019, **141**, 15693–15699.
13 L. Schmidt-Mende, A. Fechtenkötter, K. Müllen, E. Moons, R. H. Friend and J. D. MacKenzie, *Science*, 2001, **293**, 1119–1122.
14 X. L. Feng, M. Y. Liu, W. Pisula, M. Takase, J. L. Li and K. Müllen, *Adv. Mater.*, 2008, **20**, 2684–2689.
15 W. W. H. Wong, C. Q. Ma, W. Pisula, C. Yan, X. L. Feng, D. J. Jones, K. Müllen, R. A. J. Janssen, P. Bäuerle and A. B. Holmes, *Chem. Mater.*, 2010, **22**, 457–466.
16 Z. L. Zhu, J. Q. Xu, C. C. Chueh, H. B. Liu, Z. A. Li, X. S. Li, H. Z. Chen and A. K. Y. Jen, *Adv. Mater.*, 2016, **28**, 10786–10793.
17 W. Pisula, A. Menon, M. Stepputat, I. Lieberwirth, U. Kolb, A. Tracz, H. Sirringhaus, T. Pakula and K. Müllen, *Adv. Mater.*, 2005, **17**, 684–689.

18 J. L. Li, J. J. Chang, H. S. Tan, H. Jiang, X. D. Chen, Z. K. Chen, J. Zhang and J. S. Wu, *Chem. Sci.*, 2012, **3**, 846–850.
19 Z. J. Chen, A. Lohr, C. R. Saha-Möller and F. Würthner, *Chem. Soc. Rev.*, 2009, **38**, 564–584.
20 R. Weinberger and L. C. Love, *Spectrochim. Acta, Part A*, 1984, **40**, 49–55.
21 C. Feng, C. S. Lin, W. Fan, R. Q. Zhang and M. A. Van Hove, *J. Chem. Phys.*, 2009, **131**, 1–8.
22 P. Samori, A. Fechtenkötter, F. Jäckel, T. Böhme, K. Müllen and J. P. Rabe, *J. Am. Chem. Soc.*, 2001, **123**, 11462–11467.
23 W. Jin, T. Fukushima, A. Kosaka, M. Niki, N. Ishii and T. Aida, *J. Am. Chem. Soc.*, 2005, **127**, 8284–8285.
24 T. S. Navale, M. V. Ivanov, M. M. Hossain and R. Rathore, *Angew. Chem., Int. Ed.*, 2018, **57**, 790–794.
25 R. Rathore and C. L. Burns, *J. Org. Chem.*, 2003, **68**, 4071–4074.
26 W. W. H. Wong, D. Vak, T. B. Singh, S. J. Ren, C. Yan, D. J. Jones, I. I. Liaw, R. N. Lamb and A. B. Holmes, *Org. Lett.*, 2010, **12**, 5000–5003.
27 S. Setia and S. K. Pal, *ChemistrySelect*, 2016, **1**, 880–885.
28 S. Ren, C. Yan, D. Vak, D. J. Jones, A. B. Holmes and W. W. H. Wong, *Adv. Funct. Mater.*, 2012, **22**, 2015–2026.
29 W. W. H. Wong, J. Subbiah, S. R. Puniredd, B. Purushothaman, W. Pisula, N. Kirby, K. Müllen, D. J. Jones and A. B. Holmes, *J. Mater. Chem.*, 2012, **22**, 21131–21137.
30 C. Pan, K. Sugiyasu, J. Aimi, A. Sato and M. Takeuchi, *Angew. Chem., Int. Ed.*, 2014, **53**, 8870–8875.
31 J. M. Hughes, Y. Hernandez, D. Aherne, L. Doessel, K. Müllen, B. Moreton, T. W. White, C. Partridge, G. Costantini, A. Shmeliov, M. Shannon, V. Nicolosi and J. N. Coleman, *J. Am. Chem. Soc.*, 2012, **134**, 12168–12179.
32 S. D. Bergin, Z. Y. Sun, D. Rickard, P. V. Streich, J. P. Hamilton and J. N. Coleman, *ACS Nano*, 2009, **3**, 2340–2350.
33 Y. Hernandez, M. Lotya, D. Rickard, S. D. Bergin and J. N. Coleman, *Langmuir*, 2010, **26**, 3208–3213.
34 F. Cataldo, *Fullerenes, Nanotubes, Carbon Nanostruct.*, 2009, **17**, 79–84.
35 R. Goddard, M. W. Haenel, W. C. Herndon, C. Krüger and M. Zander, *J. Am. Chem. Soc.*, 1995, **117**, 30–41.
36 P. T. Herwig, V. Enkelmann, O. Schmelz and K. Müllen, *Chem. – Eur. J.*, 2000, **6**, 1834–1839.
37 Z. H. Wang, F. Dötz, V. Enkelmann and K. Müllen, *Angew. Chem., Int. Ed.*, 2005, **44**, 1247–1250.
38 M. J. Frisch, G. Trucks, H. Schlegel, G. Scuseria, M. Robb, J. Cheeseman, G. Scalmani, V. Barone, B. Mennucci and G. Petersson, *Gaussian 09, Revision D.01*, Gaussian, Inc., Wallingford, CT, 2009.
39 I. B. Berlman, *J. Phys. Chem.*, 1970, **74**, 3085–3093.
40 T. H. El-Assaad, M. Auer, R. Castaneda, K. M. Hallal, F. M. Jradi, L. Mosca, R. S. Khnayzer, D. Patra, T. V. Timofeeva, J. L. Bredas, E. J. W. List-Kratochvil, B. Wex and B. R. Kaafarani, *J. Mater. Chem. C*, 2016, **4**, 3041–3058.
41 T.-W. Lee, Y. Chung, O. Kwon and J.-J. Park, *Adv. Funct. Mater.*, 2007, **17**, 390–396.
42 T.-H. Han, Y. Lee, M.-R. Choi, S.-H. Woo, S.-H. Bae, B.-H. Hong, J.-H. Ahn and T.-W. Lee, *Nat. Photonics*, 2012, **6**, 105–110.
43 SMART, SAINT and SADABS, Bruker AXS Inc., Madison, Wisconsin, USA, 2016.
44 G. M. Sheldrick, *SADABS v 2.03*, University of Göttingen, Germany, 2002.
45 *SHELXTL v 6.10*, Bruker AXS, Inc., Madison, Wisconsin, USA, 2000.

